JOURNAL OF GEOPHYSICAL RESEARCH: ATMOSPHERES, VOL. 118, 4267–4279, doi:10.1002/jgrd.50385, 2013

Linear interference and the Northern Annular Mode response to tropical SST forcing: Sensitivity to model configuration

Christopher G. Fletcher[1] and Paul J. Kushner[2]

Received 10 October 2012; revised 8 March 2013; accepted 3 April 2013; published 28 May 2013.

[1] Interannual variability in tropical sea surface temperatures (SSTs) associated with the El Niño–Southern Oscillation is linked to teleconnections with the Northern Annular Mode (NAM). Previous work highlighted that the sign and amplitude of the NAM response to tropical SSTs are controlled by the total wave activity entering the subpolar stratosphere, which depends on the linear interference of planetary wave anomalies with the climatological stationary wave field. This study uses multiple configurations of atmospheric general circulation models to assess the robustness of these linkages to details of the tropical SST forcing and model configuration. Across 23 cases with idealized SST forcing, the amplitudes of the tropical and extratropical wave responses are found to scale approximately linearly with forcing strength. But wave amplitude alone is not sufficient to predict the NAM response. Instead, the spatial structure of the wave response (and hence the linear interference) provides the best explanation of the NAM response in all cases. Linear interference explains most of the total wave activity response even in cases with stronger nonlinear contributions, due to consistent cancellation between quasi-stationary wave nonlinearity and nonlinearity arising from transient waves. Within this limited set of experiments, there is no evidence for a consistent sensitivity of the NAM response to horizontal resolution or to vertical resolution in the stratosphere. These findings reveal that linear interference provides a robust and reproducible mechanism linking midlatitude wave responses to zonal mean circulation (NAM) responses across a wide variety of forcing cases.

Citation: Fletcher, C. G., and P. J. Kushner (2013), Linear interference and the Northern Annular Mode response to tropical SST forcing: Sensitivity to model configuration, *J. Geophys. Res. Atmos.*, *118*, 4267–4279, doi:10.1002/jgrd.50385.

1. Introduction

[2] Recent studies have established that interannual variability associated with the El Niño–Southern Oscillation (ENSO) can drive robust responses in the northern wintertime high-latitude zonal circulation [*Broennimann*, 2007; *Manzini*, 2009]. A major goal of these studies is to better understand the physical mechanisms controlling the high-latitude response to tropical forcing, with the applied aim of using such connections to improve operational seasonal-to-decadal climate predictions [*Wang et al.*, 2009]. It has become apparent that the link between ENSO and the northern high latitudes involves two main components: First, a teleconnection between the tropics and the midlatitudes (Component 1) for warm ENSO events causes a Rossby wave train to propagate poleward on a great circle [*Hoskins and Karoly*, 1981], deepens the Aleutian Low, and strengthens the Pacific-North American (PNA) pattern [*Horel and Wallace*, 1981]. Second, the strengthening of the PNA pattern, in turn, increases planetary wave propagation into the subpolar stratosphere (Component 2), where the waves dissipate, which decelerates the stratospheric polar vortex [*Garfinkel and Hartmann*, 2008].

[3] Component 1 has been studied extensively and comprises a series of dynamical interactions involving tropical diabatic heating, off-equatorial forcing of planetary waves, sensitivity to tropospheric jet structure (particularly near jet exit regions), transient eddy feedbacks, and changes to midlatitude storm tracks [see *Trenberth et al.*, 1998]. Component 1 is also known to be highly nonlinear in the strength of the tropical forcing [*Hoerling et al.*, 2001]. Component 2 has received comparatively less attention, although a consensus is emerging that contributions to anomalous fluxes of wave activity that are linear in the wave anomalies play a surprisingly large role [*DeWeaver and Nigam*, 2000; *Garfinkel and Hartmann*, 2008; *Nishii et al.*, 2009; *Fletcher and Kushner*, 2011]. In particular, for warm ENSO events, constructive linear interference between the climatological stationary waves and the midlatitude planetary wave response associated with ENSO (represented by a positive PNA pattern) increases vertical wave activity into the stratosphere. Such wave events initiate a change to the zonal mean coupled stratosphere-troposphere circulation: Perturbations

Additional supporting information may be found in the online version of this article.

[1]Department of Geography and Environmental Management, University of Waterloo, Waterloo, Ontario, Canada.
[2]Department of Physics, University of Toronto, Toronto, Ontario, Canada.

Corresponding author: C. G. Fletcher, Department of Geography and Environmental Management, University of Waterloo, 200 University Ave. W., Waterloo, ON N2L 3G1, Canada. (chris.fletcher@uwaterloo.ca)

2169-897X/13/10.1002/jgrd.50385

to the stratospheric zonal mean circulation can propagate back down into the troposphere and lead to circulation anomalies that persist there for several weeks [*Baldwin and Dunkerton*, 2001].

[4] Early investigations into ENSO effects on high latitudes using observational and reanalysis data tended to suffer from sampling limitations due to the relatively few ENSO events in the historical record [*Hamilton*, 1993]; a robust link has only recently begun to emerge [*Free and Seidel*, 2009]. Thus, to fully understand the dynamics of the high-latitude response to ENSO typically requires modeling experiments. Models are able to reproduce the two components of the teleconnection [*Hoerling and Kumar*, 2002; *Ineson and Scaife*, 2009]; however, the simulation of each component may exhibit sensitivity to model formulation. Component 1 is sensitive to the representation of tropical precipitation and deep convection, which increases in the Central and Eastern Pacific during warm ENSO events, and is the mechanism that drives wave teleconnections to the extratropics through anomalous divergence in the tropical upper troposphere [*Trenberth et al*., 1998]. Increasing model horizontal resolution typically causes large changes in simulated tropical precipitation [*Boyle and Klein*, 2010], which can lead to improvements in a model's climate simulation [*Gent et al*., 2010]. However, model biases in tropical precipitation are not necessarily improved by moving to a higher resolution [*Neale and Slingo*, 2003; *Stephenson et al*., 1998]. On the other hand, Component 2 may exhibit sensitivity to model stratospheric representation. Several authors have concluded that a model with a well-resolved stratosphere is necessary to produce a coupled stratosphere-troposphere response to ENSO [*Bell et al*., 2009; *Cagnazzo and Manzini*, 2009; *Ineson and Scaife*, 2009], while others have concluded that a vertically coherent response between the troposphere and stratosphere can be found in models without a well-resolved stratosphere [*Li et al*., 2010].

[5] In this study, we investigate ENSO high-latitude teleconnections using a suite of idealized tropical forcing simulations in several atmospheric general circulation models (AGCMs). We demonstrate that there is a direct scaling between the amplitude of the tropical forcing and the amplitude of the midlatitude wave teleconnection response (Component 1). However, we find no direct scaling between the tropical forcing and the high-latitude response; instead, we show that to explain the high-latitude response—particularly in the Northern Annular Mode (NAM) in the polar stratosphere [*Thompson and Wallace*, 2000]—requires information about the horizontal and vertical structures of the planetary waves (Component 2). *Fletcher and Kushner* [2011, henceforth FK11] imposed idealized sea surface temperature (SST) warming patterns in the tropical Pacific and Indian Oceans in a single AGCM and found opposite-signed NAM responses, which were explained by differences in the phasing, and hence linear interference, of the quasi-stationary Rossby wave response and the climatological stationary wave. Following FK11, we here use an expanded set of model configurations and SST perturbations to investigate linear and nonlinear contributions to the NAM response. In particular, we will provide a more thorough exploration of the fluctuating (transient) wave activity term (see FK11 and section 2.3). We also investigate the effect of changing model horizontal and stratospheric resolution.

[6] The article is arranged as follows. Section 2 presents details on the different AGCMs used in this study and a brief comparison of their simulated wintertime climatologies with observations. This is followed by a description of the experimental design for our idealized SST forcing cases. Section 2.1.3 presents our principal diagnostics comparing the NAM responses among our ensemble of cases; this section also includes discussion of the sensitivity to model formulation and a broader examination of nonlinear contributions to the NAM responses. Section 3 presents a summary, a discussion, and our main conclusions.

2. Methods

2.1. Description of AGCMs

2.1.1. GFDL-AM2

[7] This is the same model (the Geophysical Fluid Dynamics Laboratory-Atmospheric Model version 2) as used in FK11. Briefly, the model horizontal resolution is $2^\circ \times 2.5^\circ$ (latitude-longitude); it has 26 vertical layers with the model lid at 3 hPa. The GFDL-AM2 model incorporates the finite-volume dynamical core of *Lin* [2004] and the relaxed Arakawa-Schubert convection scheme [*Moorthi and Suarez*, 1992]. See *Anderson et al*. [2004] for details.

2.1.2. NCAR CAM

[8] We use the standard version 3 of the National Center for Atmospheric Research (NCAR) Community Atmosphere Model (CAM) described in *Collins et al*. [2006] but with the following changes: (1) The dynamical core is the same finite-volume scheme of *Lin* [2004] as in GFDL-AM2, and (2) the original convection scheme [*Zhang and McFarlane*, 1995] has been modified as described in *Neale et al*. [2008] to include convective momentum transport and a dilution approximation for the calculation of convective available potential energy. The model horizontal resolution is $1.9^\circ \times 2.5^\circ$ (latitude-longitude); it has 26 vertical layers with the model lid at 3 hPa. Despite GFDL-AM2 and CAM sharing a dynamical core, there are quite substantial differences between the simulations of these two models, owing to major differences in components such as the cloud and radiation schemes (see section 2.1.5 below).

2.1.3. CAM-Hires

[9] A selection of simulations was also conducted using the CAM model with a finer horizontal resolution of $0.9^\circ \times 1.25^\circ$. There are several configuration differences between this version and the standard CAM model. First, the spatial resolution of the lower boundary topography is increased to $0.9^\circ \times 1.25^\circ$, which impacts the surface friction and the generation of subgrid-scale orographic gravity waves. Second, there are three changes to cloud parameters: (1) The threshold for autoconversion of cold ice is halved, (2) the relative humidity threshold for stable low cloud formation is reduced by 0.005 to 0.910, and (3) the relative humidity threshold for stable high cloud formation is reduced by 0.03 to 0.77. Third, to ensure stability, the time step used in the dynamical core is a function of the horizontal resolution [*Lin*, 2004]. All other physical parameters and simulation details (physics time step, etc.) were unchanged in this version. We show below that these changes from the standard CAM moderately impact the mean climate and significantly impact the response to imposed tropical forcing.

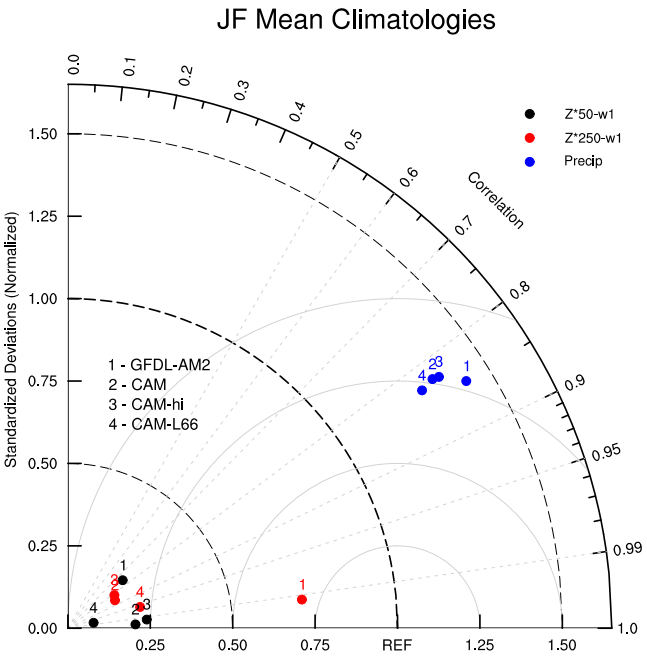

Figure 1. Taylor diagram representing the departure of January-February averages of the four AGCM control simulations from an observational climatology for tropical precipitation (blue symbols), Z^*250 hPa at 60°N for wave-1 (red symbols), and Z^*50 hPa at 60°N for wave-1 (black symbols). Observations for precipitation are computed from the Global Precipitation Climatology Project [*Adler et al*., 2003], while the Z^* data are from the National Centers for Environmental Predictions-Department of Energy (NCEP-DoE) reanalysis [*Kanamitsu et al*., 2002].

2.1.4. CAM-L66

[10] A vertically extended version of CAM with greatly improved stratospheric representation, based on the vertical levels of the Whole Atmosphere Community Climate Model [*Richter et al*., 2008], is also used. The model uses all the same physical parameters as CAM, with the exception of changes to the gravity wave drag parameterization and vertical diffusion (see *Richter et al*. [2008] for details). The simulations described in this study use fixed prescribed concentrations of radiatively active gases such as well-mixed greenhouse gases, aerosols, and ozone. We emphasize that we have disabled interactive chemistry in this version so that we can assess purely dynamical effects of improving stratospheric representation.

2.1.5. Comparison of Model Climates

[11] We compared the wintertime (January-February (JF)) mean climatologies from the unperturbed model control simulations with observational reference data (Figure 1) for metrics relevant to the NAM response to tropical SST forcing, namely, tropical precipitation and the phase and amplitude of the wave-1 stationary wave at 60°N. Simulated spatial variance of tropical (30°S–30°N) precipitation is larger than that observed, which arises from an overestimate of tropical precipitation by 25–50%—a common feature of modern general circulation models [*Lin*, 2007]—although the spatial patterns of precipitation correlate well with observations (anomaly correlation coefficients for all models are in the range 0.83–0.85).

[12] Our second performance metric is the wintertime stationary wave geopotential height at 60°N in the upper troposphere (250 hPa) and in the lower stratosphere (50 hPa). We emphasize that we evaluate the wave at 60°N, where its amplitude peaks in the lower stratosphere; this is the key region for the linear interference effects described below. The models all tend to closely reproduce the spatial structure of zonal wave number 1 (anomaly correlation coefficients all exceed 0.80). However, the models significantly underestimate the wave amplitude: In the troposphere and stratosphere, the wave-1 amplitude is less than 25% of that observed, with the exception of the tropospheric wave field in GFDL-AM2, whose amplitude is much closer to that observed. By contrast, the amplitude and spatial pattern of the extratropical zonal wave number 2 are relatively close to observations for all models (not shown). Weak stationary waves in low-top models are common and—for models with horizontal resolutions finer than about 2.5°—appear to be the result of internal atmospheric dynamics [*Boyle*, 2006]. This problem also seems to persist in our version of the high-top CAM-L66 model. The impact of these biases for tropical-extratropical teleconnections will be discussed in sections 3.2 and 4.1. In the troposphere, the wave amplitude peaks around 40°N, and in this region, we find (not shown) that the simulated stationary wave amplitudes are closer to that observed.

[13] The climatological SST fields used to drive the CAM and GFDL-AM2 models are slightly different because the GFDL-AM2 SST climatology was computed using the average 1950–1998, while the CAM SST climatology is the average 1982–2001. The resulting pattern of differences (not shown) reveals that in GFDL-AM2, the Northern Hemisphere SST anomalies are generally warmer (cooler) than those in CAM during winter (summer). The intermodel SST differences in the climatology are most pronounced over the North Pacific sector, with peak values approaching 1 K; the global mean differences are ~0.15 K. We stress that these differences exist between the GFDL-AM2 and CAM models, but in each perturbation experiment with a particular model, the same climatological SSTs are prescribed in the control and perturbation pair; thus, no SST perturbation is applied outside of the forcing region in any experiment.

2.2. Experimental Configuration

[14] Table 1 describes the 23 perturbation experiments performed for this study and lists their abbreviated titles, while Figure 2 shows the regions where SST anomalies were applied. We examine the atmospheric response to prescribed tropical SST anomalies situated in these different regions and with different signs and strengths. The experimental design is the same as in FK11; i.e., we determine the sensitivity of the high-latitude response to regional components of the full tropical SST anomaly field associated with moderate to large ENSO events. We test the separate effects of warm and cool SST anomalies associated with these events, as well as combined warming/cooling experiments that are more typical of previous studies [e.g., *Annamalai et al*., 2007; *Hoerling and Kumar*, 2002]. The emphasis is on generating a wide range of responses and examining the general behavior across a range of idealized forcings relevant to ENSO.

Table 1. Explanation of AGCM Simulations Used in This Study and Their Abbreviations Used in the Text

Abbreviation	Number of Realizations (n)	Model	Notes (Panel Showing Map in Figure S1 in the Supporting Information)
		Set 1. Pacific Warming[a]	
P	100	AM2	Blue symbols in Figures 3 and 4 (panel j)
P	100	CAM	Red symbols in Figures 3 and 4 (panel a)
Ph	100	CAM-hires	(panel d)
Ps	100	CAM-L66	(panel f)
P0.5	50	AM2	SST anomalies multiplied by 0.5 (panel r)
P1.5	90	AM2	SST anomalies multiplied by 1.5 (panel q)
Pc	100	CAM	Cooling (i.e., anomalies multiplied by −1) (panel h)
Pn34	50	AM2	SST anomalies only in Niño3.4 region (panel u)
Pn4	50	AM2	SST anomalies only in Niño4 region (panel v)
		Set 2. Indian Ocean Warming[b]	
I	100	AM2	Blue symbols in Figures 3 and 4 (panel k)
I	100	CAM	Red symbols in Figures 3 and 4 (panel b)
Ih	100	CAM-hires	(panel e)
Is	100	CAM-L66	(panel g)
I0.5	50	AM2	SST anomalies multiplied by 0.5 (panel t)
I1.5	50	AM2	SST anomalies multiplied by 1.5 (panel s)
Ic	100	CAM	Cooling (i.e., SST anomalies multiplied by −1) (panel i)
IOD	40	AM2	Indian Ocean Dipole positive phase (panel w)
		Set 3. Indo-Pacific Warming[c]	
IP	100	AM2	Blue symbols in Figures 3 and 4 (panel l)
IP	100	CAM	Red symbols in Figures 3 and 4 (panel c)
		Set 4. More Realistic Forcings[d]	
GOGA	30	AM2	Global anomalies (60°S–60°N) (panel o)
TOGA	30	AM2	All tropics (30°S–30°N) (panel n)
TWP	30	AM2	Tropical west Pacific (15°S–15°N, 120–150°E); marked "TWP" in Figure 2 (panel p)
IPF	50	AM2	Warming and cooling anomalies in Indo-Pacific sector (30°S–30°N, 40°E–75°W) (panel m)

[a]Warming anomalies associated with El Niño events imposed in the tropical Pacific (15°S–15°N, 172°E–75°W); marked "P cases" in Figure 2.
[b]Warming anomalies associated with El Niño events imposed in the tropical Indian Ocean (30°S–30°N, 40–120°E); marked "I cases" in Figure 2.
[c]Warming anomalies associated with El Niño events imposed in the tropical Indian Ocean (30°S–30°N, 40–120°E) and tropical Pacific (15°S–15°N, 172°E–75°W).
[d]Warming and cooling anomalies associated with El Niño events imposed in different tropical locations and globally (GOGA).

[15] For each model described in section 2.1, we perform a 100 year control simulation (CTRL) with fixed 1990 atmospheric composition and repeating climatological SSTs and sea ice. Starting from the 1 December restart file for each of n years of CTRL (where $30 < n < 100$), we branch a new 3 month (December-January-February (DJF)) simulation with a time-independent SST perturbation added to the climatological SSTs. This procedure creates an ensemble of n pairs of 3 month realizations from which the response is calculated as the ensemble mean of the perturbation experiment minus that of CTRL. The value of n for each perturbation experiment is shown in Table 1. As in FK11, following the switch-on perturbation, we discard the first month of output (December) to remove any spurious effects resulting from the instantaneous change in SST; thus, in the following, we focus only on the January-February (JF) mean response. The quasi-biennial oscillation, which is known to influence the high-latitude response to ENSO [*Garfinkel and Hartmann*, 2008], is not represented by any of the models, and there is no interannual variation in solar forcing. Additional details

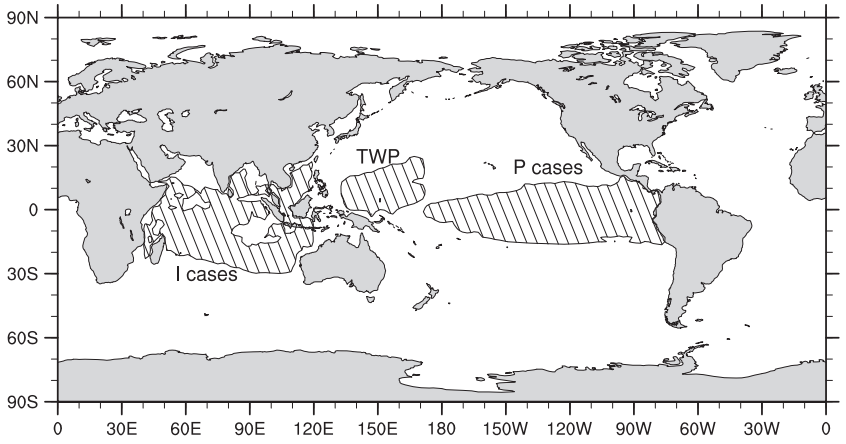

Figure 2. Hatching indicates the regions where SST perturbations are applied in the suite of cases examined in this model. The labels refer to the groups of cases listed in Table 1; also see the text for precise details of the sign and amplitude of the different forcings.

Table 2. Explanation of Diagnostics and Acronyms Used in This Study

Acronym	Notation	Diagnostic
$\lvert\Delta SST^*\rvert$		Magnitude of the zonally asymmetric tropical (30°S–30°N) SST perturbation
$\lvert\Delta OLR^*\rvert$		Magnitude of the zonally asymmetric tropical OLR response
$\lvert\Delta P^*\rvert$		Magnitude of the zonally asymmetric tropical precipitation response
$\lvert\Delta\chi^*250\rvert$		Magnitude of the zonally asymmetric tropical velocity potential response
$\lvert\Delta Z^*250\rvert$		Magnitude of the zonally asymmetric extratropical (45°N–90°N) wave response
$\Delta[Z]$-strat		Polar cap geopotential height response in the lower stratosphere (100 hPa–10 hPa)
$\Delta[Z]$-trop		Polar cap geopotential height response in the lower troposphere (1000 hPa–700 hPa)
TOTAL	$\Delta\{\langle v^*T^*\rangle\}$	Total eddy heat flux
EM_{LIN}	$\{\bar{v}_c^*\langle\Delta T^*\rangle\} + \{\langle\Delta v^*\rangle T_c^*\}$	Component of TOTAL that is linear in the eddy response
EM_{NL}	$\{\langle\Delta v^*\rangle\langle\Delta T^*\rangle\}$	Component of TOTAL that is nonlinear in the eddy response
FL	$\Delta\{\langle v^{*\prime}T^{*\prime}\rangle\}$	Component of TOTAL that represents eddy departures from the ensemble mean response

of the methodology, including maps showing the full SST perturbation field used in each of the 23 experiments, can be found in the supporting information.

[16] The prescribed SST anomalies are taken from a composite of global December-January-February anomalies of Hadley Centre Sea Ice and Sea Surface Temperature data set (HadISST) [*Rayner et al*., 2003] averaged over the five strongest warm ENSO events 1950–2001; this is the same forcing pattern shown in Figure 1 of FK11. Given the existing data set from FK11, we wanted to focus on the contrast between the cases with prescribed Indian and Pacific Ocean warming, so we repeated these "P" and "I" experiments with the three versions of CAM described in section 2.1; we also conducted an experiment with both Indian and Pacific forcings together ("IP") with the standard version of CAM. Exploring a new direction from FK11, we also assess the sensitivity to reversing the sign of the Pacific and Indian Ocean SST anomalies (i.e., prescribing a monopole cooling of the same amplitude).

2.3. Eddy Heat Flux Decomposition

[17] We diagnose linear interference based on the eddy decomposition presented in FK11 on the total eddy meridional heat flux response (perturbed minus control) $\Delta\{v^*\bar{T}^*\}$ (henceforth TOTAL; Table 2); the eddy meridional heat flux is the dominant term in the Eliassen-Palm flux into the wintertime polar stratosphere [*Newman et al*., 2001]. Similar methods have also been applied by *DeWeaver and Nigam* [2000] and *Nishii et al*. [2009]. The quantities v and T are the meridional velocity ($m\,s^{-1}$) and temperature (K), respectively. The braces around $\Delta\{\overline{v^*T^*}\}$ denote zonal averaging, the star denotes the departure from the zonal mean, and the bar denotes the January-February time mean. In the following, we use angle brackets $\langle\ldots\rangle$ to denote the ensemble average over all n realizations of an experiment. For any ensemble of realizations, TOTAL contains an ensemble and time mean term $\Delta\{\langle\bar{v}^*\rangle\langle\bar{T}^*\rangle\}$ (EM) and a fluctuating term $\Delta\{\langle\overline{v^{*\prime}T^{*\prime}}\rangle\}$ (FL) that represents the contribution to the heat flux response from the daily departures of each realization from the daily ensemble mean (denoted by the primes). Note that EM + FL ~ TOTAL: Our use of ensemble, time, and zonal averaging means that in FK11 and here, we do not consider an additional fluctuating term that represents daily departures from the time mean. The additional term contains the contribution to TOTAL from subseasonal fluxes that are consistent between ensemble members; however, its magnitude is found to be $< 1\%$ of TOTAL (not shown) and so it is omitted from the analysis.

[18] The EM term can be further decomposed into the sum of a part that is linear in the ensemble mean wave response,

$$EM_{LIN} = \{\bar{v}_c^*\langle\Delta\bar{T}^*\rangle\} + \{\langle\Delta\bar{v}^*\rangle\bar{T}_c^*\}, \quad (1)$$

and a part that is nonlinear in the ensemble mean wave response,

$$EM_{NL} = \{\langle\Delta\bar{v}^*\rangle\langle\Delta\bar{T}^*\rangle\}, \quad (2)$$

where $\bar{v}_c^*$ and $\bar{T}_c^*$ refer to the climatological background stationary wave, i.e., the n-year ensemble and time mean from the unforced control simulations. We note a difference compared to FK11 in the notation of the EM_{LIN} and EM_{NL} terms: An error was identified in the notation used in FK11 such that it was not clear that the fluxes were being computed using time mean $\bar{v}^*$ and $\bar{T}^*$. We have found (not shown) that computing the fluxes using time mean data instead of daily data strengthens EM_{LIN} and weakens the nonlinear flux (EM_{NL} + FL), each by 15–20%, because time averaging reduces the daily covariances between the anomalous v^* and T^*. However, we have verified that this effect does not impact our primary conclusions. Finally, we note that the large ensemble sizes used in the present study ensure statistical significance in all of the responses we comment on in the text.

3. Results

3.1. Dynamics of the NAM Response to Tropical SST Anomalies

[19] Across the experiments, there is an approximately proportional relationship between the magnitudes of the response of the zonally asymmetric components of tropical SST ($|\Delta SST^*|$) and tropical outgoing longwave radiation (OLR) ($|\Delta OLR^*|$; Figure 3a). Departures from this simple relationship, for example, in the "Pc" (Pacific cold) case, are expected because SSTs need to exceed thresholds to induce tropical convection [e.g., *Folkins and Braun*, 2003; *Hoerling et al*., 2001]. The simulations generally fall on a sensitivity curve corresponding to a $17\,W\,m^{-2}$ radiative anomaly per K surface warming. The OLR response represented by $|\Delta OLR^*|$ is, as expected, proportional to the magnitude of the zonally asymmetric precipitation $|P^*|$ response (Figure 3b). It is also proportional to the magnitude of the response of the 250 hPa zonally asymmetric velocity potential field $|\Delta\chi^*250|$

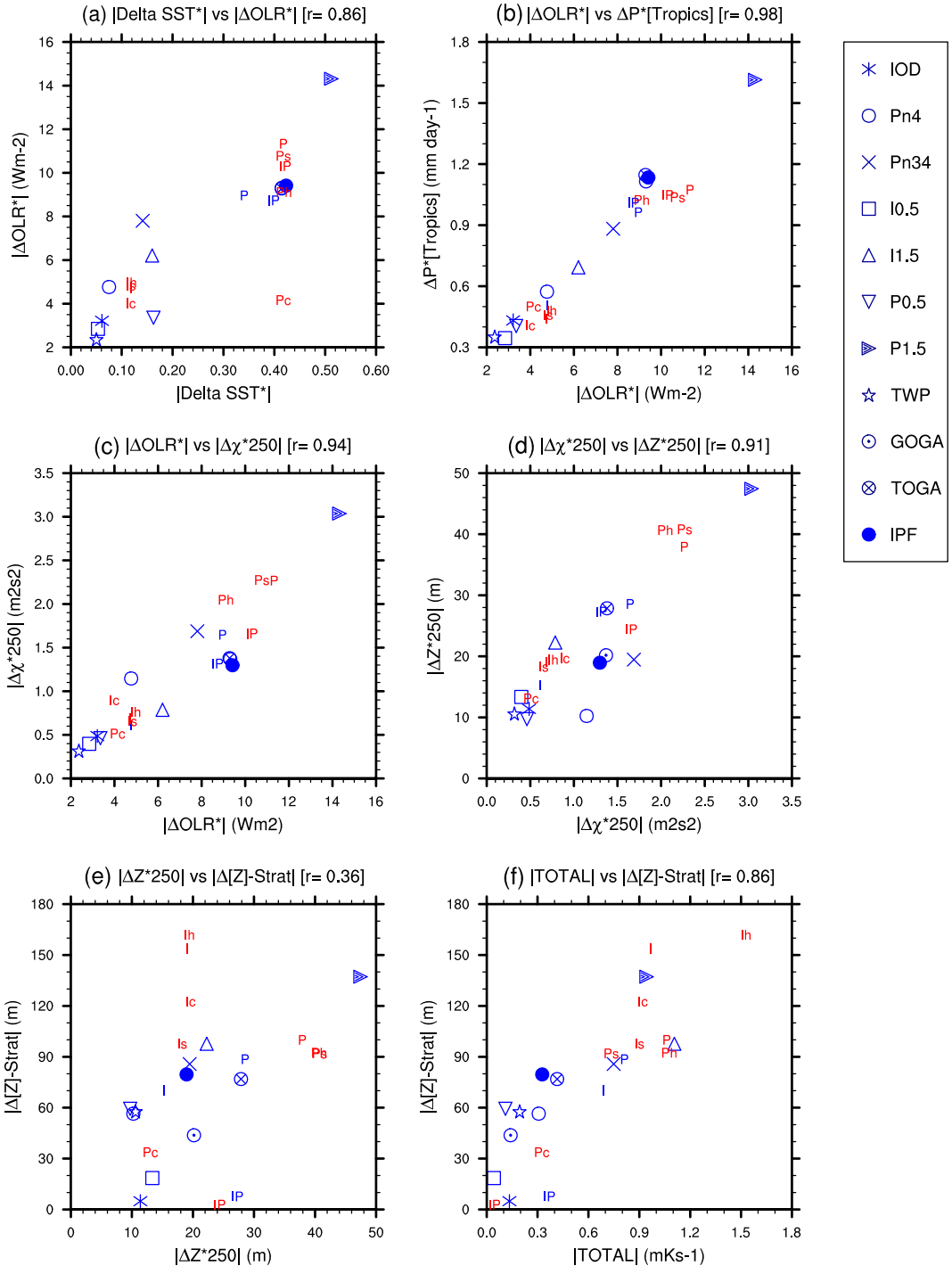

Figure 3. The relationship between the magnitudes of the tropical-extratropical wave responses among the ensemble of simulations. (a) Zonally asymmetric forcing amplitude |ΔSST*| (K) versus |ΔOLR*| ($W\,m^{-2}$); (b) |ΔOLR*| versus precipitation ($mm\,d^{-1}$); (c) |ΔOLR*| versus |Δχ*250| ($m^2\,s^2$); (d) |Δχ*250| versus |ΔZ*250| (m); (e) |ΔZ*250| versus |Δ[Z]-strat| (m); (f) |Δ[Z]-strat| versus |TOTAL| ($m\,K\,s^{-1}$). Here, and in later figures, the blue symbols show cases from the GFDL-AM2 model, while the red symbols show cases from all three configurations of the CAM model (see section 2.1). Definitions of the quantities presented are given in sections 2.3 and 3.1, and in Table 2.

(Figure 3c), which represents a measure of the large-scale divergent (irrotational) response in the tropics. In turn, the magnitude of the tropical velocity potential response |Δχ*250| is strongly correlated (Figure 3d) with the 250 hPa wave geopotential amplitude |ΔZ*250| in the extratropics between 45°N and 90°N ($r = 0.91$), indicating a clear link between the strength of the tropical forcing and the generation of extratropical waves. Across all cases, using a least squares

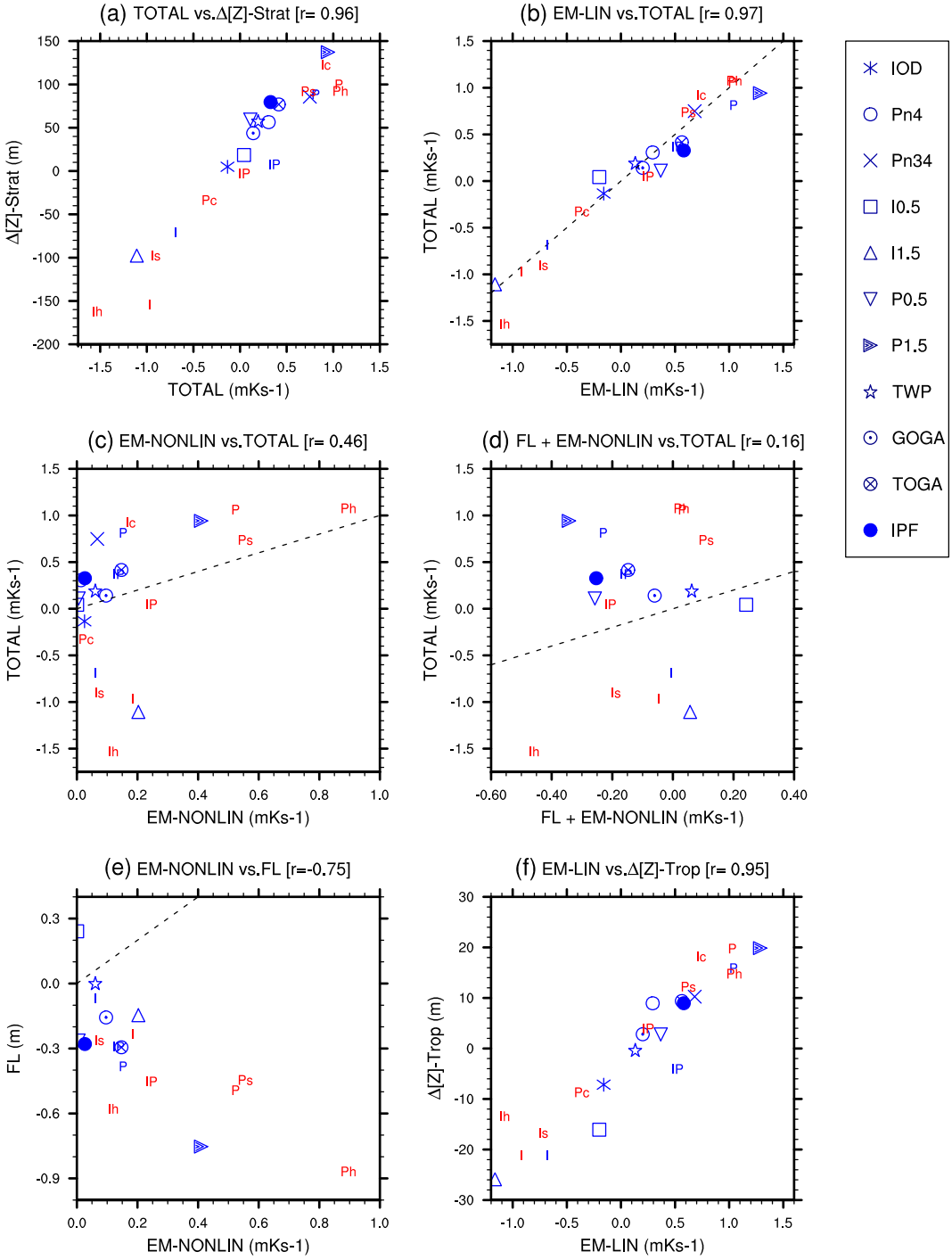

Figure 4. The relationship between measures of the extratropical wave mean flow responses among the ensemble of simulations. (a) TOTAL versus Δ[*Z*]-strat; (b) EM_{LIN} versus TOTAL; (c) EM_{NL} versus TOTAL; (d) EM_{NL} + FL versus TOTAL; (e) EM_{NL} versus FL; (f) EM_{LIN} versus Δ[*Z*]-trop. The dashed line in Figures 4b–4e shows the 1:1 relation. Definitions of the quantities presented are given in sections 2.3 and 3.1, and in Table 2. Note the values for FL were not available for the Pn3, Pn3.4, or IOD experiments.

linear fit, we obtain a scaling of 2.84 m $|\Delta Z^*250|$ per W m^{-2} $|\Delta OLR^*|$, and this scaling is similar when computed for the 14 GFDL-AM2 cases (2.72 m/W m^{-2}) and the nine CAM cases (2.96 m/W m^{-2}).

[20] Geopotential height averaged over the polar cap (60°N–90°N) between 10 hPa and 100 hPa (Δ[*Z*]-strat), which correlates strongly with the NAM response, measures the high-latitude zonal mean response. Figure 3e shows that the extratropical wave amplitude ($|\Delta Z^*250|$) is a poor predictor of |Δ[*Z*]-strat| ($r = 0.36$). This implies that additional information about the wave response is required to explain the zonal mean response. In particular, the magnitude of the total eddy meridional heat flux response (|TOTAL|; see section 2.1.1) at 40°N–80°N at 100 hPa is well correlated with the

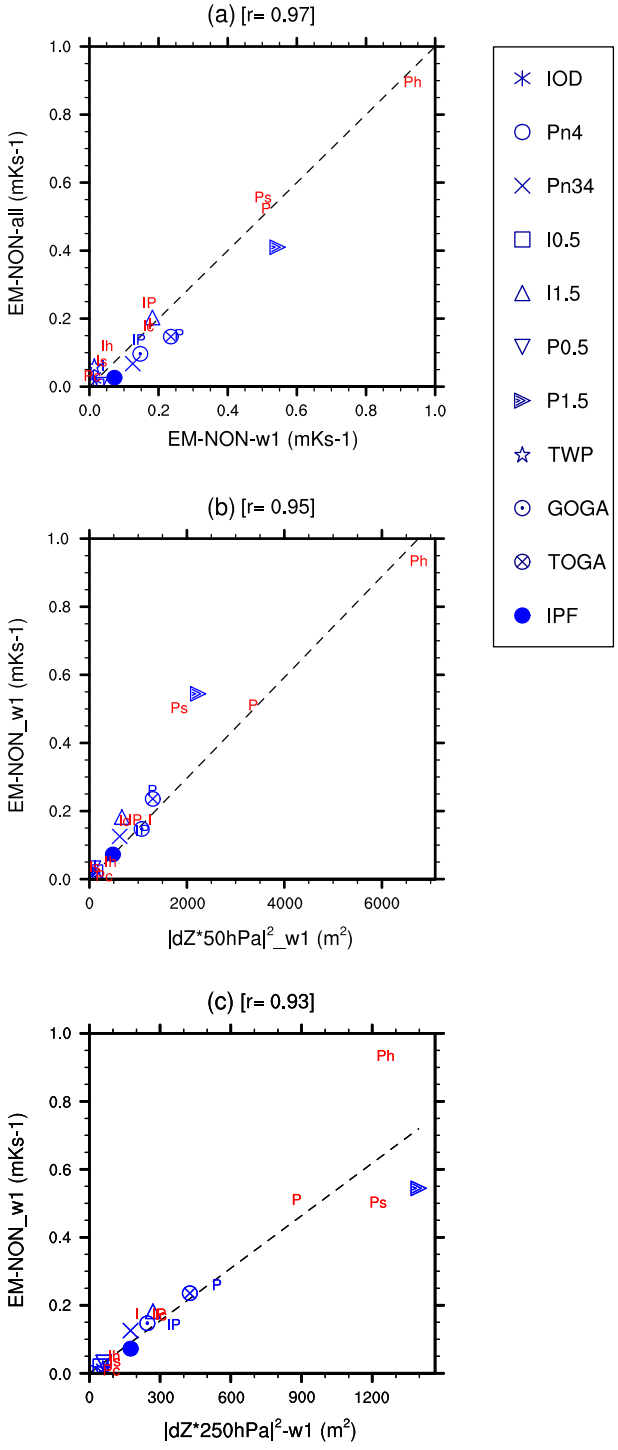

Figure 5. (a) EM_{NL} term (units m K s^{-1}; see section 2.3) for all waves plotted as a function of EM_{NL} for wave-1 only. The black dashed line indicates the 1:1 relation. The two lower panels show EM_{NL} for wave-1 against the square of the amplitude of the wave response ($|\Delta Z^*|^2$) at (b) 50 hPa and (c) 250 hPa. The black dashed lines show a linear fit that is constrained to pass through the origin. Colors and symbols are defined as in Figures 3 and 4.

amplitude of the zonal mean response $|\Delta[Z]$-strat| ($r = 0.86$; Figure 3f). In sum, stronger asymmetries in tropical SSTs ultimately lead to a strong extratropical wave response, but a stronger wave response will not lead to a proportional response in the zonal mean circulation unless it acts to change the eddy heat flux.

[21] In Figure 4, we assess the controls on $\Delta[Z]$; we start with the observation that TOTAL is an excellent predictor of both the sign and the magnitude of $\Delta[Z]$-strat (Figure 4a). In agreement with FK11, who examined a limited subset of the cases presented here, TOTAL is primarily determined by EM_{LIN} (Figure 4b), rather than by EM_{NL} (Figure 4c). The EM_{LIN} term is almost always larger than EM_{NL}, implying that TOTAL is determined by linear interference of the wave response (ΔZ^*) with the climatological stationary wave (Z^*_{climo}). The EM_{NL} term is in all cases positive, consistent with surface forcing generating an upward propagating wave activity response; in some cases (e.g., the Pacific "P" cases), it acts to reinforce EM_{LIN}, and in other cases (e.g., the Indian Ocean "I" cases), it acts to attenuate it.

[22] EM_{NL} only represents one of the nonlinear terms in the wave activity flux decomposition. The other nonlinear term, FL, represents the transient wave flux response that occurs within each realization. The FL term is generally negative and acts to cancel the EM_{NL} (Figures 4d and 4e), such that the total nonlinearity $FL + EM_{NL}$ ends up being a factor of 4 or 5 weaker than EM_{LIN}. The FL term is negative in all cases except I0.5, which is a very weak Indian Ocean forcing case that produces close to zero EM_{NL} but a relatively strong positive FL term. Evidence of this systematic cancellation was found in FK11 and has now been verified in the broader set of integrations and models considered here. Finally, we also note that the total nonlinearity measured by $|EM_{NL}| + |FL|$ tends to increase with forcing amplitude (Figure 4e). While it makes sense that the nonlinear terms should increase in size with forcing amplitude, at this point, we have no straightforward explanation for why the cancellation of the two nonlinear terms is so consistent across the ensemble of cases.

[23] The relevance of these results for tropospheric dynamics is that the linear contribution to the wave activity flux response through 100 hPa, EM_{LIN}, is proportional to the tropospheric NAM response as measured by $\Delta[Z]$-trop, which is the geopotential height averaged over the polar cap (60°N–90°N) between 1000 hPa and 700 hPa (see Figure 4f, which generalizes FK11's Figure 8 to this larger set of experiments). Linear interference produces a zonal mean circulation response that is vertically coherent from the troposphere to the stratosphere. While the GFDL-AM2 and CAM experiments exhibit similar sensitivity in Figure 4f, the ratio $\Delta[Z]$-trop/$\Delta[Z]$-strat, which is a measure of the strength of stratosphere-troposphere coupling, is 40% weaker in CAM (0.14 m/m) than in GFDL-AM2 (0.21 m/m). However, we reiterate that our ensemble of experiments in CAM and GFDL-AM2 are not identical and therefore a rigorous comparison of stratosphere-troposphere coupling for the two models cannot be performed here.

[24] Some cases stand out in their breakdown of the linear and nonlinear terms. For example, in the Pacific warming cases with the three versions of the CAM model (labeled Ph, P, and Ps), the magnitudes of the EM_{NL} and FL nonlinear terms individually approach the magnitude of EM_{LIN}. Yet, because the nonlinear terms cancel (Figure 4e), they do not play a large net role. Nonetheless, it is striking that only by accounting for the nonlinear transient eddy response represented by FL does the linear character of these cases emerge.

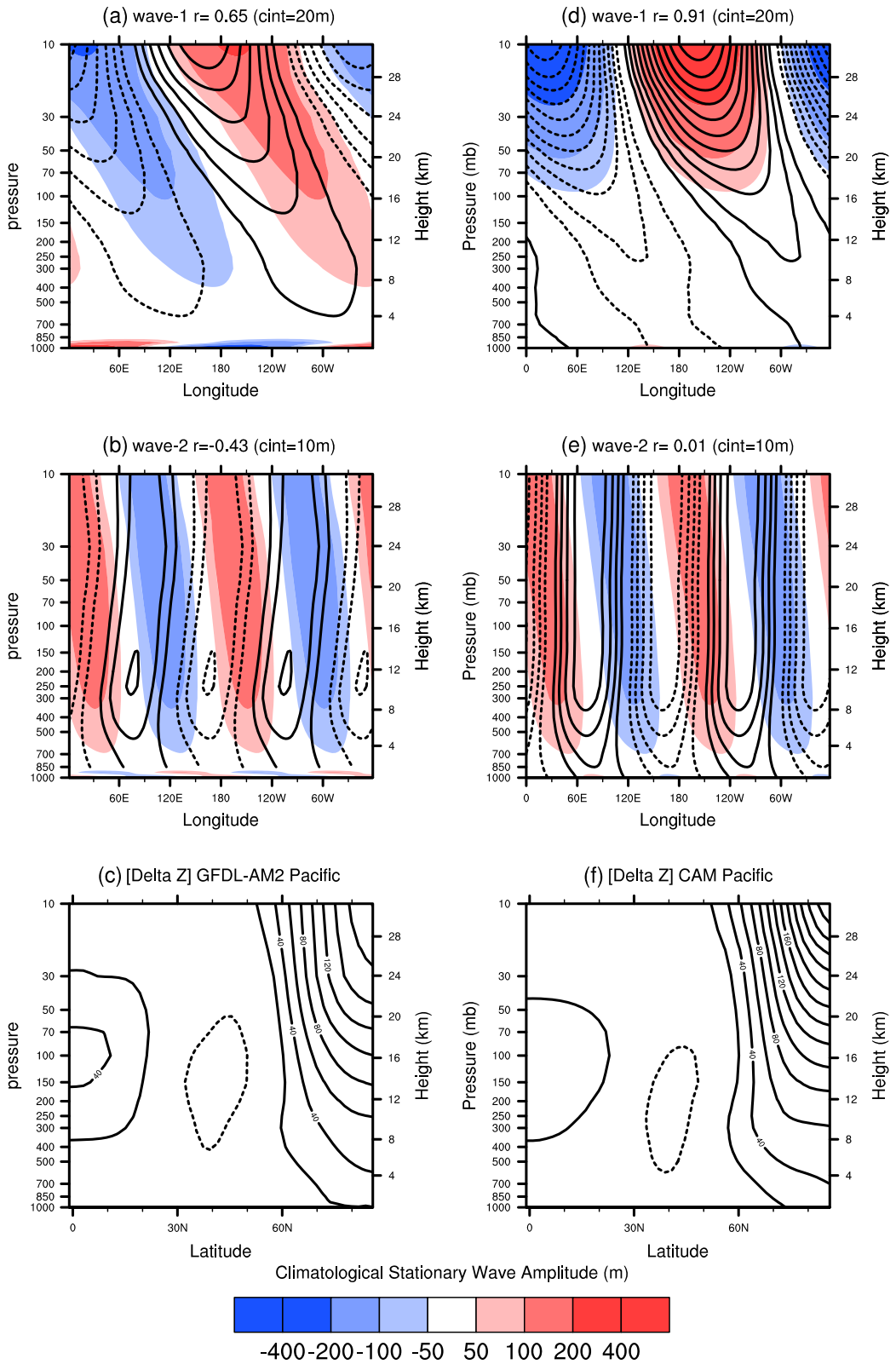

Figure 6. (a, b, d, e) Longitude-pressure sections of the wave geopotential height response at 60°N (Z*60°N) for the Pacific warming cases in (left) GFDL-AM2 and (right) CAM. The response is presented separately for the (top row) wave-1 and (middle row) wave-2 components. The wave response (ΔZ*) is shown in contours (interval is indicated in the figure caption), with dashed contours denoting negative values; the climatological stationary wave (Z^*_{climo}) is shaded. The pressure-weighted anomaly correlation between ΔZ* and Z^*_{climo} in the vertical range 100 hPa–10 hPa is shown in the title in each panel. (c, f) Zonal mean geopotential height response ($\Delta[Z]$).

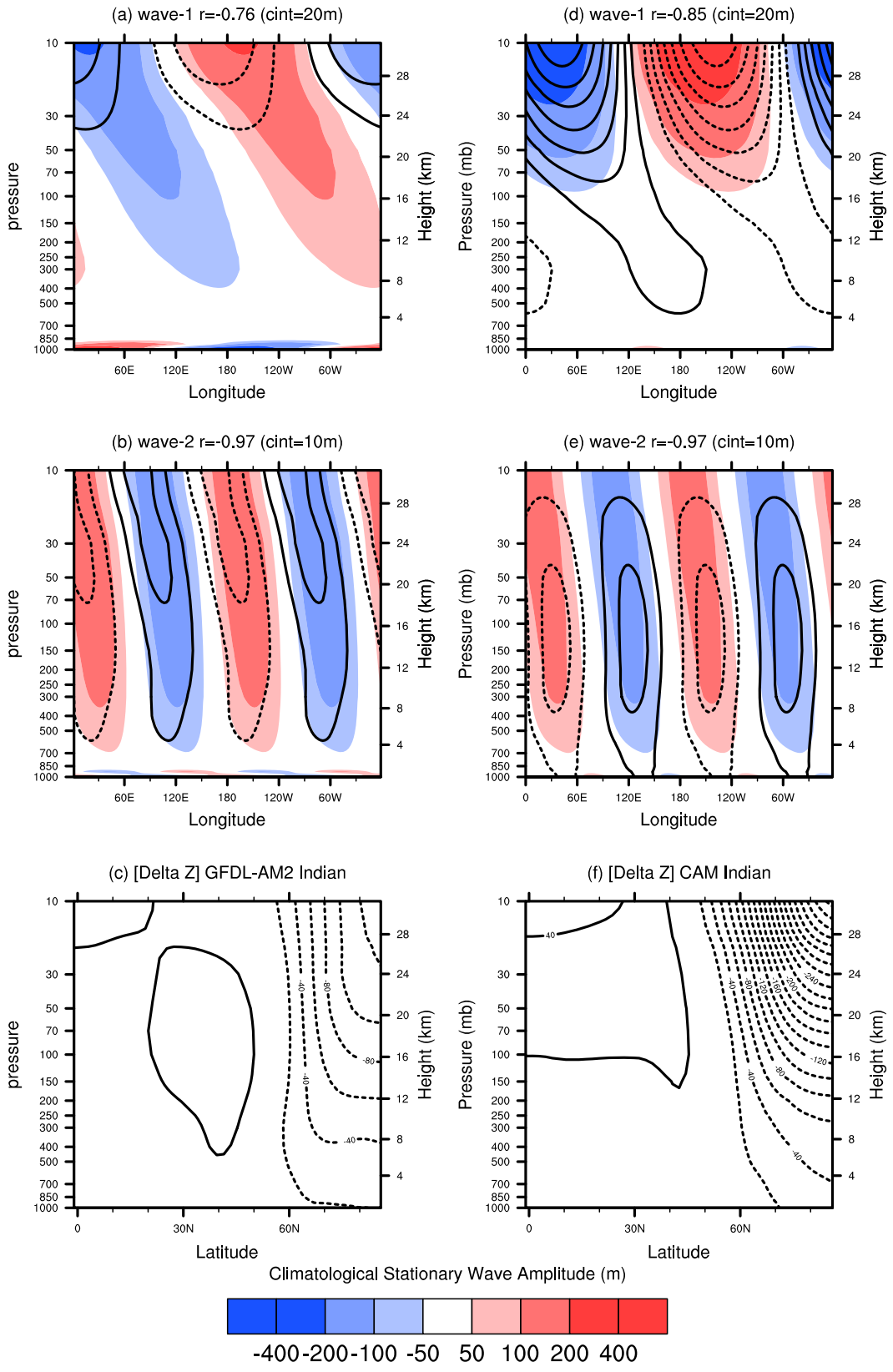

Figure 7. As in Figure 6 except for the Indian Ocean warming cases.

3.2. Sensitivity to Model Stratospheric Representation and Horizontal Resolution

[25] There is significant interest in how tropical SST anomalies affect the northern winter polar stratosphere on seasonal timescales and in the subsequent influence of the stratosphere on the troposphere [*Bell et al*., 2009; *Cagnazzo and Manzini*, 2009; *Garfinkel and Hartmann*, 2008]. The experiment pairs P/Ps and I/Is reveal no systematic impact of stratospheric representation on the stratospheric response: P/Ps produces similar $\Delta[Z]$-strat but TOTAL is 35% stronger in the low-top model, while I/Is produces similar TOTAL but $\Delta[Z]$-strat is 50% stronger in the low-top model (Figure 4a). For both experiment pairs, the responses in EM_{LIN} and $\Delta[Z]$-trop are weaker in the high-top model (Figure 4f); however, the effect on stratosphere-troposphere coupling strength is nonrobust ($\Delta[Z]$-trop/$\Delta[Z]$-strat values are 0.20/0.13 for P/Ps and 0.14/0.17 for I/Is, respectively). Thus, we cannot conclude that stratosphere-troposphere coupling is weaker in the high-top model, and our assessment from these experiments is that stratospheric representation plays only a limited role in determining the NAM response to tropical SST anomalies.

[26] Regarding the effect of horizontal resolution, experiment pairs P/Ph and I/Ih do not exhibit systematic differences in behavior in their tropical and midlatitude responses. For example, the OLR* response in Ph is somewhat weaker than that in P, but the responses are indistinguishable for I and Ih (Figure 3a) and the overall extratropical wave amplitude appears to be unaffected by horizontal resolution for both experiment pairs (Figure 3d). On the other hand, although the net nonlinearity does not exhibit a systematic difference (Figure 4d), the individual nonlinear terms FL and EM_{NL} are generally larger in magnitude for the high-resolution cases (Figure 4e), with large increases in size of the FL terms in both cases. It thus appears that higher-resolution simulations have a stronger transient eddy response to tropical forcing. Because of the cancellation between the two nonlinear terms, the impact of these sensitivities on the tropospheric response and the TOTAL response is not systematic. But, the results do suggest a potential for significant model dependence in the response to tropical forcing via the FL term.

3.3. Characteristics of the EM_{NL} Response

[27] Assuming EM_{NL} in equation (2) is controlled primarily by wave amplitude rather than by baroclinic effects due to the vertical structure of the wave response, our expectation is that EM_{NL} should scale as the square of the wave amplitude (i.e., EM_{NL} would quadruple for a doubling in wave amplitude). In Figure 5, we demonstrate this scaling across our ensemble of cases by relating EM_{NL} at 100 hPa to the square of the wave-1 amplitude ($|\Delta Z^*|^2$) at different vertical levels. We focus only on wave-1 because the all-wave EM_{NL} is clearly dominated by its wave-1 component (Figure 5a); the contribution to EM_{NL} from wave-2 is an order of magnitude smaller and displays no relationship with wave amplitude (not shown). The majority of cases show close to the expected scaling, and this relation is slightly stronger for the stratospheric wave amplitude (Figure 5b) than for the tropospheric wave amplitude (Figure 5c). The largest departures from this scaling are seen in the three cases with the strongest $|\Delta Z^*|^2$ in the troposphere (Figure 5c), which are the "P" cases with the CAM-hires and CAM-L66 models and the P1.5 case with GFDL-AM2. The "P" case in the standard CAM falls very close to the overall sensitivity line.

[28] In theory, the same scaling should apply in a single model when the forcing strength is varied; for example, in the GFDL-AM2 cases P0.5, P, and P1.5, EM_{NL} should scale with the ratio 1:4:9. Instead, we find EM_{NL} for these cases is 0.006, 0.153, and 0.410, respectively, indicating a scaling of 0.13:3.4:9. We interpret this as follows: The 3.4:9 scaling of P to P1.5 is fairly close to the predicted value of 4:9, but the 0.13:3.4 scaling of P0.5 to P is much weaker than expected. But, Figure 3a suggests that P0.5 produces a generally weak tropical response, indicating that—like the Pacific cooling case (Pc)—the SST anomaly in P0.5 is likely below the required threshold for generating a strong convective response, and this leads to the weak scaling.

3.4. Comparing the Planetary Wave Contributions in GFDL-AM2 and CAM

[29] Finally, we assess the robustness in the wave forcing of zonal responses in the CAM and GFDL-AM2 models. In Figures 6 and 7, we show that the high-latitude $\Delta[Z]$ responses are similar for cases with similar SST forcing. The Pacific warming ("P") cases have similar $\Delta[Z]$-strat and TOTAL (Figure 4a), and they also have similar EM_{LIN} and $\Delta[Z]$-trop (Figure 4f), which suggests that the wave responses in both models to the SST forcing are similar. However, it appears that the $\Delta[Z]$ responses are dynamically somewhat distinct; i.e., the two models produce similar $\Delta[Z]$ from quite different patterns of linear interference. From Figure 6a, the amplitude of wave-1 ΔZ^* in GFDL-AM2 is 50% weaker than that in CAM (Figure 6d) and the wave-2 response in GFDL-AM2 (Figure 6b) tilts more eastward with height than that in CAM (Figure 6e), suggesting a negative contribution to EM_{NL} from baroclinic effects. The Indian Ocean warming ("I") cases show similar $\Delta[Z]$-trop (Figure 4f), but $\Delta[Z]$-strat is a factor of 2 stronger in CAM than in GFDL-AM2 (Figure 4a). The decomposition of the wave response shows that in CAM, ΔZ^* is dominated more by wave-1 (Figures 7a and 7d), and the wave-2 amplitude peaks more in the troposphere in CAM and in the lower stratosphere in GFDL-AM2 (Figures 7b and 7e). These results suggest that there is no simple relationship between the strength of TOTAL and $\Delta[Z]$. Instead, to explain the TOTAL and $\Delta[Z]$ responses to tropical forcing in a particular model requires accounting for the structure of the ΔZ^* relative to Z^*_{climo}, as well as the amplitude of Z^*_{climo}. In addition, to predict $\Delta[Z]$ from TOTAL could require knowledge of the strength of each model's effective damping of wave activity. Furthermore, these factors need to be accounted for over at least the two longest zonal waves [*Garfinkel et al*., 2010].

4. Discussion

4.1. Summary

[30] We conducted an extended ensemble of experiments to examine the response of the extratropical zonal and seasonal mean circulation ($\Delta[Z]$) at northern high latitudes to prescribed tropical SST forcing. Across 23 cases with different combinations of four model configurations and 16 SST anomaly patterns (Table 1), we found a linear relationship between

the amplitude of the zonally asymmetric tropical convective heating response and the amplitude of the extratropical wave teleconnection response. Linear interference between the wave response (ΔZ^*) and the climatological stationary wave (Z^*_{climo}) was found to explain the majority of the zonal mean response $\Delta[Z]$ in the stratosphere and the troposphere. This scaling behavior is found even in cases with increased nonlinear wave activity contributions because of systematic compensation between the ensemble mean nonlinear and the transient eddy contributions to the wave activity response. Across the range of cases, the nonlinear component of stationary wave activity ($\mathrm{EM_{NL}}$) shows close to expected quadratic scaling with the amplitude of the wave response. For similar tropical SST forcing in different models, there is no simple relationship between the total wave activity and $\Delta[Z]$; instead, each model appears to have its own characteristic flavor of linear interference.

[31] Sensitivity tests revealed no systematic impact on $\Delta[Z]$ from changing model horizontal resolution, although cases conducted with the higher-resolution CAM-hires model tended to exhibit stronger nonlinearity in their wave activity responses. In contrast to *Bell et al*. [2009] and *Cagnazzo and Manzini* [2009], our experiments showed that model stratospheric representation did not have a large influence on the NAM response to tropical SST forcing. We note that the climatological stationary wave pattern in our version of the high-top model (CAM-L66) shows a similar weak bias to the low-top version of CAM (Figure 1), so it remains unclear what effect a more realistic stratospheric climatology might have on the NAM response. In other sensitivity tests, prescribing SST cooling instead of warming in the Pacific and Indian Oceans causes nonlinearity in tropical convective heating due to SST threshold effects; however, the amplitude of tropical-extratropical teleconnections in the cooling cases exhibits similar scaling to the warming cases. Indian Ocean cooling produces a very large positive $\Delta[Z]$ response, providing further evidence that SSTs in this region may drive highly nonlinear atmospheric responses [*Sardeshmukh et al*., 2000].

4.2. Conclusions

[32] There is still some uncertainty as to which parts of the wave teleconnection between the tropics and midlatitudes (referred to as Component 1 in section 1) are linear and which are nonlinear in the tropical forcing, but we have made some progress in this area. In Figure 3, we show evidence for a simple scaling between the strength of $|\Delta\mathrm{OLR}^*|$ and the magnitude of the extratropical wave response averaged over the entire extratropics 45°N–90°N ($|\Delta Z^*250|$). However, we have found (not shown) that the sign of regional features within the ΔZ^*250 pattern—for example, changes in the strength of the Aleutian Low—is extremely sensitive to the longitudinal position of maximum tropical $|\Delta\mathrm{OLR}^*|$: The group of Pacific (Indian) Ocean warming cases each produces negative (positive) height responses over the Aleutian Islands, with the sign reversal occurring abruptly for cases with $|\Delta\mathrm{OLR}^*|$ centered around 110°E. A similar finding was reported by *Barsugli et al*. [2006], but this effect warrants a more careful study, possibly using prescribed idealized SST patches applied systematically at many different longitudes. Yet, our diagnosis of the influence of the midlatitude wave response on the high-latitude zonal mean circulation (referred to as Component 2 in section 1) reveals surprisingly linear dynamics in operation across our ensemble of cases. This suggests that once a midlatitude wave response of a particular phase and amplitude is generated in the troposphere, the wave driving and $\Delta[Z]$ response in the stratosphere (and the subsequent downward propagating response into the troposphere) operate according to linear interference. This viewpoint also suggests that to understand $\Delta[Z]$, it may not be particularly important whether the wave response associated with ENSO is an externally forced PNA pattern [*Garfinkel et al*., 2010] or whether the response simply projects onto, and amplifies, the internally generated PNA pattern [*Straus and Shukla*, 2002].

[33] The extended set of cases with the CAM models provides further evidence that the wave response to Indian Ocean warming is less robust than the wave response to Pacific warming. For example, Figures 6 and 7 show that the high-latitude response in CAM is dominated by wave-1 in both cases, whereas in GFDL-AM2, the Indian Ocean case contains a larger contribution from wave-2. This suggests that the wavelength of the response to Indian Ocean forcing is somewhat dependent on the details of the model, which was also shown by *Annamalai et al*. [2007] and in the multimodel simulations presented in *SanchezGomez et al*. [2008], where two out of five models produced annular responses and the remainder produced responses that projected onto the circumglobal wave-5 pattern [*Branstator*, 2002]. One theory to explain such model dependence is the proximity of the transient eddy forcing in a given model to the location of its Asian jet core [*Li et al*., 2006], but this remains to be investigated in detail. Finally, the impact of weak biases in model stationary waves on the high-latitude response needs to be determined; further simulations using high-top models with more realistic stationary wave amplitude will likely be required.

[34] **Acknowledgments.** Computations were performed on the TCS supercomputer at the SciNet HPC Consortium. SciNet is funded by the Canada Foundation for Innovation under the auspices of Compute Canada, the Government of Ontario, Ontario Research Fund Research Excellence, and the University of Toronto [*Loken et al*., 2010]. PJK and CGF thank the Natural Sciences and Engineering Research Council of Canada for the support. We are grateful for the helpful comments received from the three anonymous reviewers.

References

Adler, R. F., et al. (2003), The version-2 Global Precipitation Climatology Project (GPCP) monthly precipitation analysis (1979–present), *J. Hydrometeor*, *4*(6), 1147–1167, doi:10.1175/1525-7541(2003)004 < 1147:TVGPCP > 2.0.CO;2.

Anderson, J. L., et al. (2004), The new GFDL global atmosphere and land model AM2-LM2: Evaluation with prescribed SST simulations, *J. Climate*, *17*(24), 4641–4673.

Annamalai, H., H. Okajima, and M. Watanabe (2007), Possible impact of the Indian Ocean SST on the Northern Hemisphere circulation during El Niño, *J. Climate*, *20*(13), 3164–3189.

Baldwin, M. P., and T. P. Dunkerton (2001), Stratospheric harbingers of anomalous weather regimes, *Science*, *294*, 581–584.

Barsugli, J. J., S. I. Shin, and P. D. Sardeshmukh (2006), Sensitivity of global warming to the pattern of tropical ocean warming, *Climate Dyn.*, *27*(5), 483–492.

Bell, C. J., L. J. Gray, A. J. Charlton-Perez, M. M. Joshi, and A. A. Scaife (2009), Stratospheric communication of El Niño teleconnections to European winter, *J. Climate*, *22*(15), 4083–4096.

Boyle, J. S. (2006), Upper level atmospheric stationary waves in the twentieth century climate of the Intergovernmental Panel on Climate Change simulations, *J. Geophys. Res.*, *111*(D14), D14101, doi:10.1029/2005JD006612.

Boyle, J., and S. A. Klein (2010), Impact of horizontal resolution on climate model forecasts of tropical precipitation and diabatic heating for the TWP-ICE period, *J. Geophys. Res.*, *115*, D23113, doi:10.1029/2010JD014262.

Branstator, G. (2002), Circumglobal teleconnections, the jet stream waveguide, and the North Atlantic Oscillation, *J. Climate*, *15*(14), 1893–1910.

Broennimann, S. (2007), Impact of El Niño Southern Oscillation on European climate, *Rev. Geophys.*, *45*(2), RG3003, doi:10.1029/2006RG000199.

Cagnazzo, C., and E. Manzini (2009), Impact of the stratosphere on the winter tropospheric teleconnections between ENSO and the North Atlantic and European region, *J. Climate*, *22*(5), 1223–1238.

Collins, W. D., P. J. Rasch, B. A. Boville, J. J. Hack, J. R. McCaa, D. L. Williamson, B. P. Briegleb, C. M. Bitz, S. J. Lin, and M. Zhang (2006), The formulation and atmospheric simulation of the Community Atmosphere Model version 3 (CAM3), *J. Climate*, *19*(11), 2144–2161.

DeWeaver, E., and S. Nigam (2000), Do stationary waves drive the zonal-mean jet anomalies of the northern winter? RID A-8338-2009, *J. Clim.*, *13*(13), 2160–2176, doi:10.1175/1520-0442(2000)013 < 2160:DSWDTZ 2.0.CO;2.

Fletcher, C. G., and P. J. Kushner (2011), The role of linear interference in the annular mode response to tropical SST forcing, *J. Climate*, *24*(3), 778–794, doi:10.1175/2010JCLI3735.1.

Folkins, I., and C. Braun (2003), Tropical rainfall and boundary layer moist entropy, *J. Climate*, *16*(11), 1807–1820, doi:10.1175/1520-0442(2003) 016 < 1807:TRABLM > 2.0.CO;2.

Free, M., and D. J. Seidel (2009), Observed El Niño–Southern Oscillation temperature signal in the stratosphere, *J. Geophys. Res.*, *114*, D23108, doi:10.1029/2009JD012420.

Garfinkel, C. I., and D. L. Hartmann (2008), Different ENSO teleconnections and their effects on the stratospheric polar vortex, *J. Geophys. Res.*, *113*(D18), D18114, doi:10.1029/2008JD009920.

Garfinkel, C. I., D. L. Hartmann, and F. Sassi (2010), Tropospheric precursors of anomalous Northern Hemisphere stratospheric polar vortices, *J. Climate*, *23*(12), 3282–3299.

Gent, P. R., S. G. Yeager, R. B. Neale, S. Levis, and D. A. Bailey (2010), Improvements in a half degree atmosphere/land version of the CCSM, *Clim. Dyn.*, *34*(6), 819–833, doi:10.1007/s00382-009-0614-8.

Hamilton, K. (1993), An examination of observed Southern Oscillation effects in the Northern Hemisphere stratosphere, *J. Atmos. Sci.*, *50*(20), 3468–3474, doi:10.1175/1520-0469(1993)050 < 3468:AEOOSO > 2.0.CO;2.

Hoerling, M. P., and A. Kumar (2002), Atmospheric response patterns associated with tropical forcing, *J. Climate*, *15*(16), 2184–2203.

Hoerling, M. P., A. Kumar, and T. Xu (2001), Robustness of the nonlinear climate response to ENSO's extreme phases, *J. Climate*, *14*(6), 1277–1293, doi:10.1175/1520-0442(2001)014 < 1277:ROTNCR > 2.0.CO;2.

Horel, J. D., and J. M. Wallace (1981), Planetary-scale atmospheric phenomena associated with the Southern Oscillation, *Mon. Wea. Rev.*, *109*(4), 813–829.

Hoskins, B. J., and D. Karoly (1981), The steady linear response of a spherical atmosphere to thermal and orographic forcing, *J. Atmos. Sci*, *38*, 1179–1196.

Ineson, S., and A. A. Scaife (2009), The role of the stratosphere in the European climate response to El Niño, *Nature Geo.*, *2*(1), 32–36.

Kanamitsu, M., W. Ebisuzaki, J. Woollen, S.-K. Yang, J. J. Hnilo, M. Fiorino, and G. L. Potter (2002), NCEP-DOE AMIP-II Reanalysis (R-2), *Bull. Amer. Meteor. Soc.*, *83*(11), 1631–1643, doi:10.1175/BAMS-83-11-1631.

Li, S., M. Hoerling, S. Peng, and K. Weickmann (2006), The annular response to tropical Pacific SST forcing, *J. Climate*, *19*(9), 1802–1819.

Li, S., J. Perlwitz, M. Hoerling, and X. Chen (2010), Opposite annular responses of the Northern and Southern Hemispheres to Indian Ocean warming, *J. Climate*, *23*(13), 3720–3738, doi:10.1175/2010JCLI3410.1.

Lin, S. J. (2004), A "vertically Lagrangian" finite-volume dynamical core for global models, *Mon. Wea. Rev.*, *132*(10), 2293–2307.

Lin, J.-L. (2007), The double-ITCZ problem in IPCC AR4 coupled GCMs: Ocean-atmosphere feedback analysis, *J. Climate*, *20*(18), 4497–4525, doi:10.1175/JCLI4272.1.

Loken, C., et al. (2010), SciNet: Lessons learned from building a power-efficient top-20 system and data centre, *J. Phys. Conf.*, *256*, 012026, doi:10.1088/1742-6596/256/1/012026.

Manzini, E. (2009), Atmospheric science ENSO and the stratosphere, *Nat. Geosci.*, *2*(11), 749–750, doi:10.1038/ngeo677.

Moorthi, S., and M. Suarez (1992), Relaxed Arakawa-Schubert—A parameterization of moist convection for general-circulation models, *Mon. Weather Rev.*, *120*(6), 978–1002, doi:10.1175/1520-0493(1992) 120 < 0978:RASAPO > 2.0.CO;2.

Neale, R., and J. Slingo (2003), The maritime continent and its role in the global climate: A GCM study, *J. Clim.*, *16*(5), 834–848, doi:10.1175/1520-0442(2003)016 < 0834:TMCAIR > 2.0.CO;2.

Neale, R. B., J. H. Richter, and M. Jochum (2008), The impact of convection on ENSO: From a delayed oscillator to a series of events, *J. Climate*, *21*(22), 5904–5924.

Newman, P. A., E. R. Nash, and J. E. Rosenfield (2001), What controls the temperature of the Arctic stratosphere during the spring?, *J. Geophys. Res.*, *106*(D17), 19999–20010.

Nishii, K., H. Nakamura, and T. Miyasaka (2009), Modulations in the planetary wave field induced by upward-propagating Rossby wave packets prior to stratospheric sudden warming events: A case-study, *Q. J. R. Meteorol. Soc.*, *135*(638), 39–52, doi:10.1002/qj.359.

Rayner, N. A., D. E. Parker, E. B. Horton, C. K. Folland, L. V. Alexander, D. P. Rowell, E. C. Kent, and A. Kaplan (2003), Global analyses of sea surface temperature, sea ice, and night marine air temperature since the late nineteenth century, *J. Geophys. Res.*, *108*(D14), 4407, doi:10.1029/2002JD002670.

Richter, J. H., F. Sassi, R. R. Garcia, K. Matthes, and C. A. Fischer (2008), Dynamics of the middle atmosphere as simulated by the Whole Atmosphere Community Climate Model, version 3 (WACCM3), *J. Geophys. Res.*, *113*, D08101, doi:10.1029/2007JD009269.

SanchezGomez, E., C. Cassou, D. L. R. Hodson, N. Keenlyside, Y. Okumura, and T. Zhou (2008), North Atlantic weather regimes response to Indian-western Pacific Ocean warming: A multi-model study, *Geophys. Res. Lett.*, *35*(15), L15706, doi:10.1029/2008GL034345.

Sardeshmukh, P. D., G. P. Compo, and C. Penland (2000), Changes of probability associated with El Niño, *J. Climate*, *13*(24), 4268–4286, doi:10.1175/1520-0442(2000)013 < 4268:COPAWE > 2.0.CO;2.

Stephenson, D. B., F. Chauvin, and J. F. Royer (1998), Simulation of the Asian summer monsoon and its dependence on model horizontal resolution, *J. Meteorol. Soc. Jpn.*, *76*(2), 237–265.

Straus, D. M., and J. Shukla (2002), Does ENSO force the PNA?, *J. Climate*, *15*(17), 2340–2358.

Thompson, D. W. J., and J. M. Wallace (2000), Annular modes in the extratropical circulation. Part I: Month-to-month variability*, *J. Climate*, *13*(5), 1000–1016, doi:10.1175/1520-0442(2000)013 < 1000:AMITEC 2.0.CO;2.

Trenberth, K. E., G. W. Branstator, D. Karoly, A. Kumar, N. C. Lau, and C. Ropelewski (1998), Progress during TOGA in understanding and modeling global teleconnections associated with tropical sea surface temperatures, *J. Geophys. Res.*, *103*, 14291–14324.

Wang, B., et al. (2009), Advance and prospectus of seasonal prediction: Assessment of the APCC/CliPAS 14-model ensemble retrospective seasonal prediction (1980–2004), *Clim. Dyn.*, *33*(1), 93–117, doi:10.1007/s00382-008-0460-0.

Zhang, G. J., and N. A. McFarlane (1995), Sensitivity of climate simulations to the parameterization of cumulus convection in the Canadian Climate Centre general circulation model, *Atmosphere-Ocean*, *33*(3), 407–446.